

See discussions, stats, and author profiles for this publication at: <https://www.researchgate.net/publication/23184722>

EPR and Mössbauer Spectroscopy of Intact Mitochondria Isolated from Yah1p-Depleted *Saccharomyces cerevisiae* †

ARTICLE *in* BIOCHEMISTRY · OCTOBER 2008

Impact Factor: 3.02 · DOI: 10.1021/bi801047q · Source: PubMed

CITATIONS

41

READS

56

9 AUTHORS, INCLUDING:



[Marlène Martinho](#)

Aix-Marseille Université

31 PUBLICATIONS 803 CITATIONS

[SEE PROFILE](#)



[E. Ann Ellis](#)

Texas A&M University

106 PUBLICATIONS 1,582 CITATIONS

[SEE PROFILE](#)



[Roland Lill](#)

Philipps University of Marburg

202 PUBLICATIONS 14,869 CITATIONS

[SEE PROFILE](#)

EPR and Mössbauer Spectroscopy of Intact Mitochondria Isolated from Yah1p-Depleted *Saccharomyces cerevisiae*[†]

Ren Miao,[‡] Marlène Martinho,[§] Jessica Garber Morales,[‡] Hansoo Kim,^{||} E. Ann Ellis,^{||} Roland Lill,[⊥] Michael P. Hendrich,[§] Eckard Münck,[§] and Paul A. Lindahl*,^{‡,§,#}

Department of Chemistry, Texas A&M University, College Station, Texas 77843-3255, Department of Chemistry, Carnegie Mellon University, Pittsburgh, Pennsylvania 15213-2683, Microscopy and Imaging Center, Texas A&M University, College Station, Texas 77843-3255, Institut für Zytobiologie, Philipps-Universität Marburg, Robert-Koch-Strasse 6, D-35033 Marburg, Germany, and Department of Biochemistry and Biophysics, Texas A&M University, College Station, Texas 77843

Received June 3, 2008; Revised Manuscript Received July 14, 2008

ABSTRACT: Yah1p, an [Fe₂S₂]-containing ferredoxin located in the matrix of *Saccharomyces cerevisiae* mitochondria, functions in the synthesis of Fe/S clusters and heme *a* prosthetic groups. EPR, Mössbauer spectroscopy, and electron microscopy were used to characterize the Fe that accumulates in Yah1p-depleted isolated intact mitochondria. Gal-YAH1 cells were grown in standard rich media (YPD and YPGal) under O₂ or argon atmospheres. Mitochondria were isolated anaerobically, then prepared in the as-isolated redox state, the dithionite-treated state, and the O₂-treated state. The absence of strong EPR signals from Fe/S clusters when Yah1p was depleted confirms that Yah1p is required in Fe/S cluster assembly. Yah1p-depleted mitochondria, grown with O₂ bubbling through the media, accumulated excess Fe (up to 10 mM) that was present as 2–4 nm diameter ferric nanoparticles, similar to those observed in mitochondria from *yfh1Δ* cells. These particles yielded a broad isotropic EPR signal centered around *g* = 2, characteristic of superparamagnetic relaxation. Treatment with dithionite caused Fe³⁺ ions of the nanoparticles to become reduced and largely exported from the mitochondria. Fe did not accumulate in mitochondria isolated from cells grown under Ar; a significant portion of the Fe in these organelles was in the high-spin Fe²⁺ state. This suggests that the O₂ used during growth of Gal-YAH1 cells is responsible, either directly or indirectly, for Fe accumulation and for oxidizing Fe²⁺ → Fe³⁺ prior to aggregation. Models are proposed in which the accumulation of ferric nanoparticles is caused either by the absence of a ligand that prevents such precipitation in wild-type mitochondria or by a more oxidizing environment within the mitochondria of Yah1p-depleted cells exposed to O₂. The efficacy of reducing accumulated Fe along with chelating it should be considered as a strategy for its removal in diseases involving such accumulations.

A substantial portion of cellular Fe metabolism occurs in mitochondria. This includes the import of Fe ions from the cytosol, the assembly of iron–sulfur (Fe/S) clusters, the biosynthesis of hemes, the insertion of these Fe prosthetic groups into mitochondrial apoproteins, and the regulation of these processes. The past decade has witnessed substantial advances in understanding the biochemical players involved in these processes (1–4).

Cytosolic Fe²⁺ ions are transported into the matrix compartment of the mitochondria via inner membrane

(IM)¹ transporters, including (but probably not limited to) Mrs3p and Mrs4p (5). Once in the matrix, the yeast frataxin homologue 1 (Yfh1p) accepts Fe²⁺ ions either directly from these transporters or from unknown intermediary Fe-donors (1). Some evidence suggests that Yfh1p delivers Fe²⁺ ions to scaffold proteins Isu1p/Isu2p in the matrix for subsequent Fe/S cluster assembly. Yfh1p may deliver Fe²⁺ ions to isolated ferrochelatase for heme biosynthesis (3), but the

[†] This study was supported by the Robert A. Welch Foundation (A1170, P.A.L.), National Science Foundation Grant MCB-0424494 (E.M.), National Institutes of Health Grant GM77387 (M.P.H.), Deutsche Forschungsgemeinschaft (SFB 593, Gottfried-Wilhelm Leibniz program), Fonds der chemischen Industrie (R.L.) and the Chemistry Biology Interface training program (J.G.M.).

* To whom correspondence should be addressed. Phone: 979-845-0956. Fax: 979-845-4719. E-mail: lindahl@mail.chem.tamu.edu.

[‡] Department of Chemistry, Texas A&M University.

[§] Department of Chemistry, Carnegie Mellon University.

^{||} Microscopy Imaging Center, Texas A&M University.

[⊥] Philipps-Universität Marburg.

[#] Department of Biochemistry and Biophysics, Texas A&M University.

¹ Abbreviations: YAH1 and Yah1p, gene and protein, respectively, of yeast adrenodoxin homologue 1; Gal-YAH1, a genetic construction in which a galactose-inducible promoter replaces the natural YAH1 promoter; YPD, yeast peptone dextrose growth media; YPGal, same as YPD but with galactose replacing dextrose; Yah1p-depleted/O₂, Gal-YAH1 cells grown on YPD under O₂; Yah1p-replete/O₂, Gal-YAH1 cells grown on YPGal under O₂; Yah1p-depleted/Ar, Gal-YAH1 cells grown on YPD under argon; IM, inner mitochondrial membrane; ISC, Fe/S cluster; EPR, electron paramagnetic resonance; DNPH, 2,4-dinitrophenylhydrazine; EM, electron microscopy; TEM, transmission electron microscope; STEM, scanning transmission electron microscope; HAADF, high angle annular dark field; EDX, energy dispersive X-ray; OD, optical density; EGTA, glycol-bis(2-aminoethyl ether)-N,N,N',N'-tetraacetic acid; PVDF, polyvinylidene fluoride; TBS buffer, 20 mM Tris, 0.9% NaCl, pH 7.5; ICP-MS, inductively coupled plasma emission mass spectrometry; WT, wild-type; E/D, EPR rhombicity parameter; T_B, blocking temperature; ΔE_Q, quadrupole splitting; δ, isomer shift.

physiological meaning of this is uncertain (6, 7). After Fe/S clusters are assembled on Isu1p/Isu2p, chaperone proteins Jac1p and Ssq1p and the monothiol glutaredoxin Grx5p (8) facilitate the transfer of Fe/S clusters to mitochondrial Fe/S apoproteins. The Fe/S cluster (ISC) assembly machinery further assists in the synthesis of an unknown species that is exported to the cytosol via the ABC type IM transporter Atm1p, where it serves to mature cytosolic Fe/S proteins.

In 1999, Barros and Nobrega (9) identified open reading frame *YPL252C* in *Saccharomyces cerevisiae* as the homologue to human adrenodoxin and named it *Yeast Adrenodoxin Homologue 1* (*Yah1*). Human adrenodoxin is an [Fe₂S₂]-cluster-containing protein that works with ferredoxin reductase to transfer electrons from NADPH to a mitochondrial P450 involved in the synthesis of pregnenolone (9).

Lange et al. (10) discovered that Yah1p localizes to the mitochondrial matrix and is required for mitochondrial ISC assembly. By exchanging the natural promoter of *YAH1* with a galactose-inducible promoter, *YAH1* expression levels in the strain Gal-*YAH1* could be controlled according to carbon source. When Gal-*YAH1* cells are grown on glucose, Yah1p is depleted, ISC biosynthesis is diminished significantly, and Fe accumulates. Yah1p and Arh1p may function together to provide electrons for ISC assembly, but this has not been established. Yah1p may also function to maintain Fe in the Fe²⁺ oxidation state (8). The extent of Fe accumulation is time-dependent (10), suggesting that Yah1p-depleted cells cannot regulate Fe in mitochondria as well as wild type (WT) cells.

Yah1p is involved in the assembly of the respiratory complexes. Barros et al. (11, 12) found that Yah1p is involved in heme *a* biosynthesis. They identified a hydroxylation reaction catalyzed by the monooxygenase Cox15p, using electrons donated by Yah1p and Arh1p.

Iron also accumulates in other strains of *S. cerevisiae* that lack various proteins involved in mitochondrial ISC metabolism, most notably Yfh1p (13). Based on Mössbauer spectroscopy and chemical analysis, Lesuisse et al. assigned the Fe that accumulates in mitochondria from *yfh1*/Δ cells to ferric phosphate nanoparticles (14). The accumulated Fe may render these organelles hypersensitive to oxidants and promote formation of reactive oxygen species (15).

In humans, a deficiency of frataxin causes the neurodegenerative disease Friedreich's ataxia (16, 17). Current therapy includes ingesting Fe³⁺ chelators, but this has met with only modest success (18). The pathogenesis of the disease has received considerable attention, and a general though not universal consensus has emerged. Frataxin might be a matrix-bound Fe carrier, accepting Fe²⁺ ions from IM transporters and donating them to proteins that serve as entry points for Fe/S protein biosynthesis. Thus, a deficiency of this protein might inhibit this transport, leading to the absence of Fe/S prosthetic groups (14, 17). Iron probably accumulates because feedstock Fe²⁺ ions continue to be delivered into the matrix in the absence of frataxin.

Depletion of Yah1p causes Fe to accumulate in mitochondria, and it impairs Fe/S cluster (10) and heme *a* (11) biosynthesis. Since a biophysical characterization of the Fe accumulating in Yah1p-depleted strains has been lacking, we report here on the use of EPR and Mössbauer spectroscopy to establish that the Fe which accumulates in the Gal-*YAH1* mutant is aggregated as high-spin Fe³⁺ nanoparticles.

We found that Fe/S cluster synthesis is significantly reduced in Yah1p-depleted mitochondria while our results regarding heme biosynthesis are less certain. We qualitatively assess the conditions responsible for Fe accumulation, determine how much Fe accumulates, evaluate the oxidation state and magnetic properties of the accumulated Fe, and show that the accumulated Fe is not chemically inert but can be reduced to the Fe²⁺ state by dithionite. Electron microscopy is employed to visualize these particles, and mechanistic chemical models are presented to help explain their formation.

EXPERIMENTAL PROCEDURES

Yeast Strains and Media. The published *S. cerevisiae* strain Gal-*YAH1* (*MAT α, ura3-1, ade2-1, trp1-1, his3-11,15, leu2-3,112*) carrying a galactose-inducible promoter instead of the natural promoter of *YAH1* was used (10). Cells were grown on standard rich medium (1% yeast extract, 2% peptone) supplemented with the required carbon source (2% glucose for YPD or 2% galactose for YPGal) until the OD(600) was 0.7–1.1. To prevent foaming, 100 ppm silicone antifoam B (JT Baker) was added to the media. To enrich samples with ⁵⁷Fe, a 10-fold molar excess of sodium citrate was added to ⁵⁷Fe³⁺ ions in acid (final pH ~5.5) and this solution was added to the media to obtain a final ⁵⁷Fe concentration of ~40 μM.

Growth and Harvesting Condition. Cells were grown in a 25 L glass fermenter at 30 °C, as described (19). For aerobic growth, pure O₂ was bubbled through the media at a flow rate of ~2 L/min. For anaerobic growth, the media was supplemented with 20 mg/L ergosterol (Acros Organics) and 1.0 mL/L Tween-80 (Acros Organics) dissolved in 1.0 mL/L ethanol, which was sterilized by heating for 10 min in boiling water. Research-grade (99.998% pure) argon (Botco Co., TX, USA) was used for anaerobic cell growth to maintain anaerobiosis. For this growth, media was vigorously deaerated by bubbling with Ar for 1 h before inoculation; thereafter the flow rate was set at ~2 L/min. Approximately 50 mL of aerobically cultured cells at OD(600) ~ 1 was used as the inoculum, requiring cells to undergo 8–10 mass doublings before harvesting (when OD(600) = 0.7–1.1) to ensure complete anaerobic adaptation.

Aerobically grown cells were harvested by centrifugation (5 min at 5000g) and then transferred to an Ar-atmosphere glovebox (MBraun) maintained at ~6 °C and ~1 ppm of O₂. Anaerobically grown cells were transferred (through PharMed tubing driven by a peristaltic pump) into an Ar-atmosphere glovebox (Vacuum Atmospheres Inc., O₂ < 3 ppm) while the culture in the reactor was continuously bubbled with Ar at a flow rate > 15 L/min. The suspension culture was transferred into sealed centrifuge bottles, removed from the box and centrifuged as above. The bottles were then returned to the box, and the process was repeated. Thus, anaerobically grown cells were not exposed to significant O₂ during either growth or harvesting.

Mitochondria Isolation and Treatments. Mitochondria were isolated as described (19) except for the following modifications. Lyticase (Sigma; 300 units/g wet weight cells) was used to form spheroplasts within 1 h. Spheroplasts were gently ruptured in a glass Dounce homogenizer (tight fitting, 20–40 strokes). Cell debris was removed at 1500g for 5 min, and the soluble mitochondria fraction was pelleted at 12000g

for 10 min. Resulting crude mitochondria were further purified using a discontinuous 16–22% Nycodenz (Sigma) gradient at 150000g for 1 h. As determined by electron microscopy (EM) the interface of two layers contained mitochondria. This layer was collected and will be referred to as intact mitochondria in the as-isolated state. As-isolated mitochondria were further characterized by O₂ consumption measurements as described (19).

Portions of as-isolated mitochondrial samples were packed by centrifugation at 15000g for 2 h into EPR or Mössbauer holders and frozen in liquid N₂ for subsequent analysis, essentially as described (19). EPR and Mössbauer spectra were collected, analyzed, and simulated as described (19). There was some batch-to-batch variation in the extent of ⁵⁷Fe incorporation into mitochondria. Prior to packing, some aliquots of as-isolated mitochondria were incubated for 1 h with 5 mM sodium dithionite in a buffer containing 0.6 M sorbitol, 100 mM Tris (pH 8.5) and 1 mM EGTA. Other aliquots were incubated with 1 atm O₂ for 30 min before packing and freezing.

Western Blots. Cellular extracts were prepared as described (20), and 20 μL portions were separated by SDS-PAGE and transferred onto polyvinylidene fluoride (PVDF) membranes (Bio-Rad). Membranes were blocked by nonfat milk (5%) in TBS buffer (20 mM Tris, 0.9% NaCl, pH 7.5) and 0.1% Tween 20 before protein detection. An ECL Western blotting detection kit (Amersham Biosciences) was used to detect Yah1p-antisera as visualized using a Fujifilm LAS-3000 imaging system.

Oxyblot Assay. The assay was performed using an Oxyblot kit (Millipore, USA) following manufacturer's procedures. Isolated mitochondria were solubilized with 12% SDS, derivatized with 2,4-dinitrophenylhydrazine (DNPH) and separated on a 4–20% SDS-PAGE gel. The primary antibody used for the Western blot was raised against DNPH.

Protein and Metal Analysis. Mitochondrial protein concentrations were determined by the Biuret method (21), correcting for turbidity (22). The relative error due to turbidity caused a 10–30% overestimate of protein concentration. Metal analysis was performed using a DRCII ICP-MS spectrometer (Perkin-Elmer). Typically three volumes (50 μL, 75 μL and 100 μL) of mitochondrial suspensions were digested in sealed plastic tubes in 100 μL of 70% trace-metal grade nitric acid (Fisher Scientific) at 95 °C overnight. Digested samples were diluted with deionized and distilled H₂O to a final HNO₃ concentration of 0.2 M before measurement.

Electron Microscopy. Mitochondrial pellets were fixed in 3% (vol/vol) glutaraldehyde in isolation medium, washed with isolation medium and treated overnight at 4 °C with 1% para-phenylenediamine (wt/vol) in isolation buffer followed by dehydration in a graded methanol series to propylene oxide. Pellets were then infiltrated and embedded in epoxy resin followed by polymerization overnight at 60 °C. Ultrathin sections (100 nm) were cut with an ultramicrotome and picked up on copper grids. Grids were stabilized with a 10 nm deposit of carbon before examination in the transmission electron microscope.

Elemental analysis was performed on a TECNAI F20 (scanning) transmission electron microscope (TEM/STEM) fitted with a Schottky field emission gun, a high angle annular dark field (HAADF) detector, and an Oxford instruments

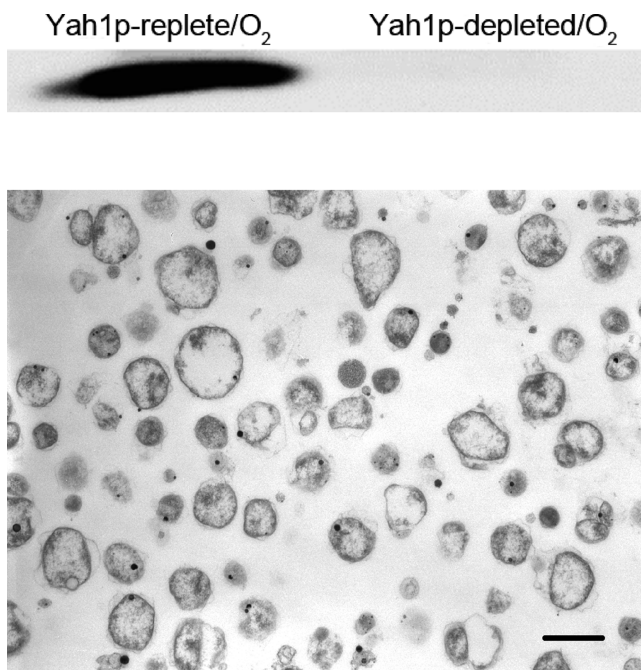


FIGURE 1: Image characterization of mitochondria. Top panel: Western blot of *S. cerevisiae* Gal-YAH1 crude extract; left, Yah1p-replete/O₂; right, Yah1p-depleted/O₂. Bottom panel: Electron micrographs of Yah1p-replete/O₂ mitochondria collected from a Nycodenz gradient. Sections were post stained with uranyl acetate and lead citrate. Bar = 1 μm.

ultrathin window energy dispersive X-ray spectroscopy (EDX) detector. The combination of STEM and EDX allows direct imaging of a nanoscale area and *in situ* identification of component elements. An EDX spectrum at each spot in the area of interest was collected at a 200 kV accelerating voltage and a ~15° tilting angle with a stationary electron probe in STEM mode. An elemental map was then acquired after choosing a proper energy window for an element-specific transition along with STEM-HAADF images.

Mössbauer and EPR Spectroscopy. Most Mössbauer spectra were collected at Carnegie Mellon University, with two spectrometers, using Janis Research Super-Varitemp dewars that allowed studies in applied magnetic fields up to 8.0 T in the temperature range from 1.5 to 200 K. Some Mössbauer spectra were also collected at Texas A&M University, using a model MS4 WRC spectrometer (WEB Research, Edina, MN) with a 4.5 to 300 K closed-cycle helium refrigerated system and a W106 temperature controller. Data from both instruments were analyzed using the WMOSS software package (WEB Research, Edina, MN). Isomer shifts are quoted relative to Fe metal at 298 K. EPR spectra were recorded on an X-band Bruker EMS spectrometer with an Oxford ESR900 liquid He cryostat. Quantitative analysis of EPR spectra used *SpinCount* (M. Hendrich) with CuEDTA as the spin standard. Spectra were recorded with a modulation amplitude of 1 mT at 100 kHz, and if used for concentration determination, under nonsaturating microwave power conditions.

RESULTS

S. cerevisiae Gal-YAH1 cells allow the expression of YAH1 to be controlled by the carbon source used in the growth media. Cells grown under standard fermenting

Table 1: Analytical Characterization of Mitochondria Isolated from *S. cerevisiae* Gal-YAH1 Cells^a

	Fe (μM)	Cu (μM)	Mn (μM)	Zn (μM)	O ₂ consumption (nmol of O ₂ /min/mg of protein)	protein (mg/mL)
Yah1p-replete/O ₂	1190 \pm 100	110 \pm 30	35 \pm 5	240 \pm 15	11	81 \pm 10
Yah1p-depleted/O ₂	7400 \pm 400	50 \pm 15	70 \pm 10	480 \pm 35	3	90 \pm 6
Yah1p-depleted/Ar	1250 \pm 350	40 \pm 5	10 \pm 5	540 \pm 70	ND ^b	83 \pm 8

^a Metal and protein values are for packed samples in which the volume due to external solvent (assumed to be 90% (19)) has been removed, and corrections due to turbidity effects were included. For O₂ consumption, the estimated relative error was 20%. ^b ND: Not determined.

conditions, using glucose as a carbon source (YPD media) and with O₂ bubbling through the media, will be called *Yah1p-depleted/O₂*. Such conditions repress the synthesis of Yah1p. Cells grown equivalently but using galactose as a carbon source will be called *Yah1p-replete/O₂*. These cells synthesize Yah1p and serve as the control for our experiments. Western blot analysis (Figure 1, top panel) indicates that Yah1p is effectively absent in Yah1p-depleted/O₂ cell extracts (right) but is present in Yah1p-replete/O₂ extracts (left). Cells grown on glucose (YPD media) but anaerobically under an Ar atmosphere will be called *Yah1p-depleted/Ar*.

Analytical Characterization. Mitochondria were isolated anaerobically as described in Experimental Procedures, with 1 mM EGTA included in all buffers. EM images (Figure 1, lower panel) confirmed the purity of the isolated mitochondria. Mitochondria isolated from Yah1p-replete/O₂ cells consumed O₂ at a rate (Table 1) corresponding to 5–10% of that observed using mitochondria isolated from WT yeast cells grown under respiratory conditions (19). This reduced activity may have arisen because the strain used here (W303) differed from that used by Hudder et al. (19) (D273-10B) (23). Cells grown on galactose are in a mixed respiration–fermentation mode (24) whereas cells grown on lactate, the carbon source used by Hudder et al. (19), are entirely in respiration mode. These differences are likely to have lowered the relative rate of O₂ consumption in the Yah1p-replete/O₂ mitochondria used in this study.

The rate of O₂ consumption for Yah1p-depleted/O₂ mitochondria (Table 1) was lower still. The rate could have been higher with galactose because it is a derepressing sugar, i.e., it induces respiration. The reduced rate of O₂ consumption for Yah1p-depleted/O₂ mitochondria is consistent with previous results (10) showing that Fe/S cluster assembly is impaired when Yah1p is depleted such that respiratory complexes should be largely absent or inoperative.

Metal and protein concentrations of these tightly packed samples were determined (Table 1). Fe concentrations in mitochondria isolated from Yah1p-replete/O₂ and Yah1p-depleted/Ar cells were the same within the uncertainties of the measurements ($\sim 1.2 \pm 0.3$ mM). This is either equivalent to, or somewhat higher than, the average Fe concentration in mitochondria from WT respiring cells (0.8 ± 0.2 mM) (19). In contrast, the Fe concentration in mitochondria isolated from Yah1p-depleted/O₂ cells was far higher (namely, 7.4 ± 0.4 mM), indicating significant Fe accumulation. Assuming that Fe is regulated within the mitochondria, the regulatory mechanism seems to malfunction in the absence of Yah1p, but only when Yah1p-depleted cells are grown under O₂.

Depleting cells of Yah1p had little effect on protein concentration in the mitochondria, but doing so did influence mitochondrial Cu, Mn, and Zn concentrations, lowering [Cu]

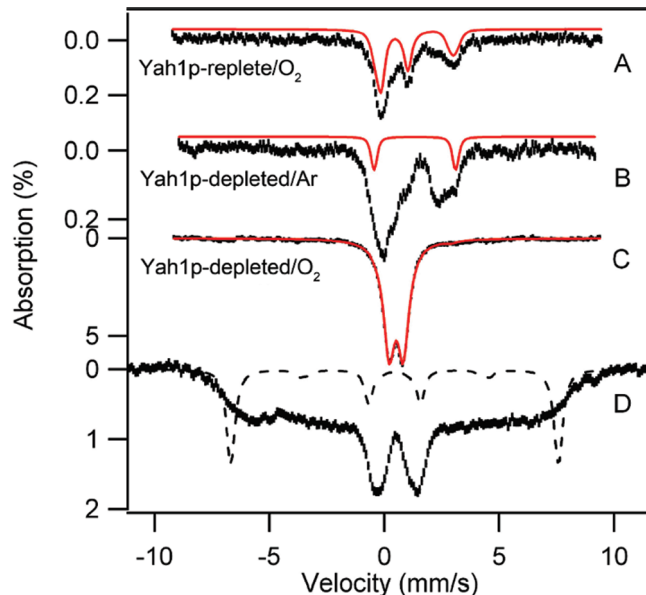


FIGURE 2: 4.2 K Mössbauer spectra of Gal-YAH1 mitochondria samples. (A) Yah1p-replete/O₂ mitochondria. The solid red line outlines the sum of two major doublets, representing 70% of the iron. (B) Yah1p-depleted/Ar mitochondria. The doublet drawn above the data outlines a high-spin ferrous species with $\Delta E_Q = 3.55$ mm/s and $\delta = 1.33$ mm/s. (C) Yah1p-depleted/O₂ mitochondria. The solid red line is a quadrupole doublet with $\Delta E_Q = 0.62$ mm/s and $\delta = 0.52$ mm/s. (D) Yah1p-replete/O₂ mitochondria of (C) studied in an 8.0 T parallel field. If the material of (C) would represent magnetically isolated Fe³⁺ ions, one would expect a spectrum as outlined by the dashed black line; for the simulation we used $A/g_\text{n}\beta_\text{n} = -21$ T for the ⁵⁷Fe magnetic hyperfine coupling constant (this A-value is appropriate for ferric phosphate).

~ 2 -fold, and raising [Mn] and [Zn] ~ 2 -fold (Table 1). Growing Yah1p-deleted cells anaerobically had little effect on [Cu] or [Zn], relative to the equivalent cells grown aerobically, but [Mn] was reduced ~ 7 -fold under these conditions. The majority of Mn ions in the mitochondria appear to be bound to Sod2p; the expression of *sod2* has been reported to be reduced by a similar factor under anaerobic growth conditions (25).

Mössbauer and EPR Spectroscopy of Yah1p-Replete/O₂ Mitochondria. Isolated intact mitochondria were either packed directly into Mössbauer and EPR sample holders (yielding the *as-isolated* state) or packed after treatment with a reductant (sodium dithionite at pH 8.5 for ~ 1 h) or an oxidant (1 atm of pure O₂ for ~ 30 min exposure). These latter states will be called *dithionite-treated* and *O₂-treated*, respectively.

As-isolated mitochondria from Yah1p-replete/O₂ cells exhibited 4.2 K Mössbauer spectra (Figure 2A) similar to those of WT mitochondria grown under aerobic respiring conditions (19), in the sense that there are two major doublets, with $\Delta E_Q \approx 1.15$ mm/s; $\delta \approx 0.45$ mm/s (roughly

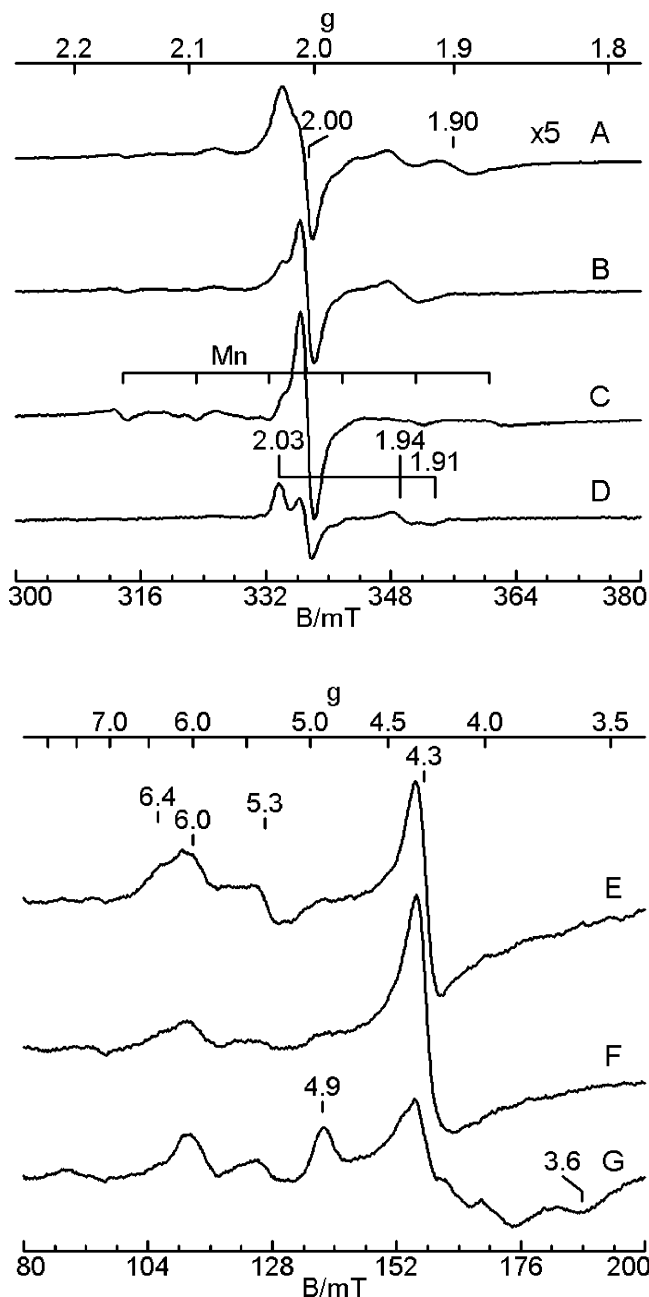


FIGURE 3: High-field (top) and low-field (bottom) EPR spectra of mitochondria isolated from Gal-YAH1 cells grown under various conditions and prepared in the as-isolated state. (A, B, E) Yah1p-replete/O₂; (C, F) Yah1p-depleted/O₂; (D, G) Yah1p-depleted/Ar. EPR parameters: temperature, 10 K; microwaves, 9.46 GHz, 20 mW (A, E-G), 0.2 mW (B-D).

40% of Fe) and $\Delta E_Q \approx 3.3$ mm/s; $\delta \approx 1.35$ mm/s (roughly 30% of Fe). These doublets belong to (predominantly) [Fe₄S₄]²⁺ clusters and high-spin Fe²⁺, respectively. The superposition of these two doublets is outlined by the solid line drawn above the data.

Yah1p-replete/O₂ mitochondria prepared in the as-isolated state exhibited three EPR signals in the high-field region (Figure 3A,B). One signal was isotropic with $g = 2.005$, the second was rhombic ($g = 2.03, 1.94$, and 1.91) with $g_{av} = 1.94$, and the third was from aqua-Mn²⁺ with $g = 2.00$ and a magnetic hyperfine constant $a = 9$ mT. Quantitative analysis indicated spin concentrations of $1.2 \mu\text{M}$ ($g_{av} = 1.94$) and $1 \mu\text{M}$ (Mn). The first signal may arise from a radical species, while the second probably originates from the

[Fe₂S₂]¹⁺ cluster of succinate dehydrogenase (19). At higher power (Figure 3A), an additional resonance is observed at $g = 1.90$, which likely arises from the Rieske [Fe₂S₂]¹⁺ cluster from cytochrome bc₁ ($g = 2.03, 1.90, 1.76$), with the other resonances obscured by other species. The concentration of the [Fe₂S₂]¹⁺ cluster of succinate dehydrogenase from the Yah1p-replete/O₂ sample is reduced by an order of magnitude relative to mitochondria obtained from WT cells grown under respiring conditions (19). This is consistent with the significantly lower O₂ consumption observed for Yah1p-replete/O₂ mitochondria. As discussed above, such differences may be caused by differences in cell strain and/or growth conditions.

In the low-field region, as-isolated Yah1p-replete/O₂ mitochondria exhibited two EPR signals that arise from high-spin ferric hemes (Figure 3E). These signals contribute at $g_{x,y} = 6.4, 5.3$ (E/D = 0.022) and $g_{\perp} = 6.0$ (E/D = 0), with spin concentrations of $0.6 \mu\text{M}$ and $0.3 \mu\text{M}$, respectively. Previously we have assigned both signals to a partially reduced state of the $a:a_3$ active site of cytochrome c oxidase in which heme a_3 is high-spin Fe³⁺ and Cu_b is in the 1+ state (19). The presence of these signals and the Fe/S signals in the $g = 2$ region indicates that Gal-YAH1 cells synthesize Fe/S clusters and heme centers when grown under conditions in which Yah1p is induced. The signal at $g = 4.3$ is from a high-spin, nonheme Fe³⁺ species with rhombic symmetry (E/D $\sim 1/3$); it has a spin concentration of less than $1 \mu\text{M}$. We cannot identify the coordination environment of such species from its EPR signal alone, but it is likely dominated by oxygen or nitrogen donor atoms.

Mössbauer and EPR Spectroscopy of Yah1p-Depleted/O₂ Mitochondria. The 4.2 K Mössbauer spectra of as-isolated mitochondria from Yah1p-depleted/O₂ cells (sample A, Figure 2C) were fundamentally different from those of Yah1p-replete/O₂ cells. The spectrum of Figure 2C exhibits a single quadrupole doublet with $\delta \approx 0.52(2)$ mm/s, $\Delta E_Q \approx 0.62(3)$ mm/s (line width $\Gamma \approx 0.55$ mm/s, full width at half-maximum). The sample did not contain any Fe²⁺. The observation of a broadened quadrupole doublet at 4.2 K, rather than a spectrum exhibiting paramagnetic hyperfine structure, indicates the presence of aggregated ferric ions. The doublet of Figure 2C was essentially identical to that observed for the *S. cerevisiae* (frataxin) deletion strain *yfh1Δ*. Based also on chemical analysis and (unpublished) EXAFS data, Lesuisse and co-workers have assigned the doublet of mitochondria from *yfh1Δ* cells to ferric phosphate nanoparticles (14).

Although sample A and the Yah1p-replete/O₂ sample described above were prepared and packed similarly into Mössbauer cuvettes, the spectral intensities of these samples differed significantly. On this basis, the ⁵⁷Fe concentration of the Yah1p-depleted/O₂ sample was roughly 10 times higher than that of the Yah1p-replete/O₂ sample, indicating that ferric ions accumulate in this mutant under aerobic growth conditions when Yah1p is depleted. This result is congruent with the analogous Fe concentrations determined by ICP-MS (see above). Using Mössbauer spectroscopy, we found no evidence for ferric nanoparticles in the Yah1p-replete/O₂ sample of Figure 2A.

Figure 2D shows a Mössbauer spectrum of sample A recorded at 4.2 K in an applied magnetic field of 8.0 T. While the largest magnetic splitting observed is reminiscent of high-

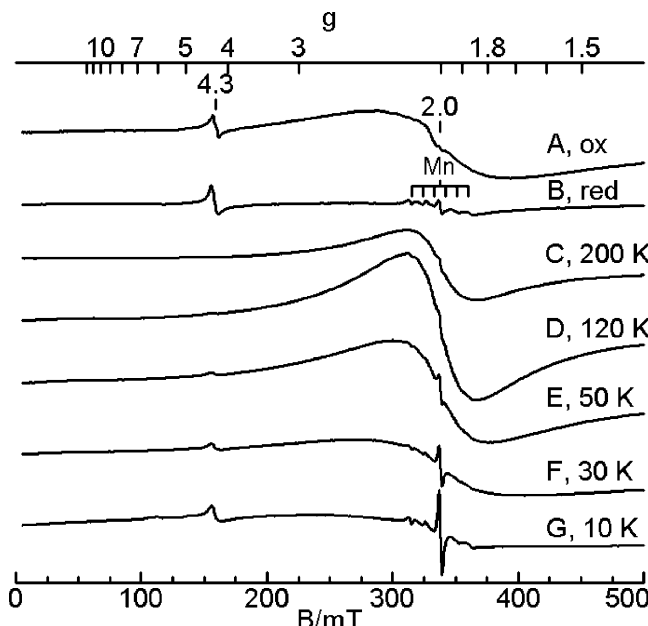


FIGURE 4: EPR spectra of Yah1p-depleted/O₂ mitochondria collected at different temperatures and in different redox states: (A) oxidized, 30 K; (B) reduced 30 K; (C–G) as-isolated, recorded at stated temperatures. EPR conditions: microwaves, 9.46 GHz, 20 mW.

spin Fe³⁺, the overall spectral shape reflects a distribution of magnetic hyperfine fields typically associated with a heterogeneous distribution of ferric nanoparticles. Although we do not fully understand the origin of these spectral features, some aspects are apparent. First, if the Fe yielding the doublet of Figure 2C were mononuclear nonaggregated Fe³⁺ (e.g., the type of iron yielding $g = 4.3$ or $g = 6$ EPR resonances), the 8.0 T spectrum would closely resemble the theoretical curve indicated by the dashed line. The spectrum of Figure 2D is readily synthesized by summing *ca.* 5 spectra of high-spin ferric species with different ⁵⁷Fe magnetic hyperfine coupling constants, corresponding to hyperfine fields from ≈ 10 to 52 T; however, in the absence of a physical model that considers very small, disordered nanoparticles that elaborate heterogeneous exchange interactions, such fits are not meaningful. Second, for ferromagnetically or antiferromagnetically ordered polycrystalline materials well-defined 6-line patterns can be observed below the Curie or Néel point (e.g., crystalline ferric phosphate is an antiferromagnet yielding a sharp 6-line spectrum at 4.2 K (26)). For nanoparticles an additional phenomenon is observed. As the temperature of the nanoparticles is raised, the thermal energy becomes comparable to the energy required to flip the bulk magnetic moment of the nanoparticle, giving rise to superparamagnetic relaxation; e.g. see ref 27. For sufficiently fast flip rates (roughly $> 10^8$ s⁻¹) the ⁵⁷Fe magnetic hyperfine interactions average to zero and a quadrupole doublet is observed. In a population of nanoparticles with variable size, the smaller particles produce a quadrupole doublet at lower temperature. The temperature at which half of the iron in the sample exhibits a quadrupole doublet is called the blocking temperature T_B . The blocking temperature is specific to the time scale of measurement; e.g. T_B (Mössbauer) $<$ T_B (EPR). For the nanoparticles of Figure 2C,D the blocking temperature must be well below 4.2 K, similar to an iron component observed in *Mycoplasma capricolum* cells (28). At 4.2 K, the latter exhibits a doublet

identical to that observed in Figure 2C. The *M. capricolum* iron component has a blocking temperature near 2 K and yields a reasonably well-defined 6-line pattern at $T = 0.07$ K. However, the *M. capricolum* magnetic hyperfine field, $B_{hf} \approx 43$ T, is distinctly smaller than the largest, and main, component, $B_{hf} = -52$ T, of the spectrum of Figure 2D, suggesting that the iron components observed for *M. capricolum* and Yah1p-depleted/O₂ cells differ despite their identical ΔE_Q and δ values.

Microcrystalline ferric nanoparticles often yield characteristic EPR spectra with features distinctly different from those observed for magnetically isolated Fe³⁺ ions (29, 30). Therefore, we have examined a Yah1p-depleted/O₂ sample with variable temperature EPR to search for such characteristics. A set of X-band spectra obtained at different temperatures is shown in Figure 4. Most prominent is a broad feature centered around $g = 2$. Such features have been shown to originate from fast thermal fluctuations of the magnetization of nanoparticles (referred to as superparamagnetic relaxation as it involved the magnetic moment of the entire particle) that average out anisotropic interactions. (For antiferromagnets the bulk magnetic moments result from uncompensated sublattice magnetizations.) Thus, this type of resonance is best observed at higher temperatures; at lower temperatures the thermal fluctuations are reduced and the amplitude of the $g \approx 2$ resonance declines, as observed here. The detailed shapes of the resonances depend strongly on shape and size distributions and on the magnetic properties of the particles. For the present study it is sufficient to note that the broad features around $g = 2$ are characteristic of superparamagnetic relaxation and present in the same state for which we observed the “nanoparticle” Mössbauer spectra of Figure 2C,D.

Other EPR Features of Mitochondria from Yah1p-Depleted/O₂ Cells. Although the focus of this study is on the superparamagnetic nanoparticles just described, mitochondria from Yah1p-depleted/O₂ cells exhibited other EPR features that contribute to their characterization. At 10 K, as-isolated Yah1p-depleted/O₂ mitochondria exhibited a 50% increase of the radical signal at $g = 2.005$ (Figure 3C) relative to that in the Yah1p-replete/O₂ sample, and the concentration of the aqua-Mn²⁺ species (4 μ M) increased 4-fold. The broad nanoparticle signal is less evident in Figure 3C than in Figure 4 due to lower microwave power and reduced sweep width. The $g_{av} = 1.94$ signal was not detectable, indicating a significant decrease in the Fe/S clusters, and consistent with lower synthesis of these clusters in Yah1p-depleted/O₂ cells. This supports previous reports that Yah1p is required for Fe/S cluster assembly (10).

The low-field region of mitochondrial samples isolated from Yah1p-depleted/O₂ cells shows the same signal at $g = 4.3$ (Figure 3F) and at the same concentration as that observed in Yah1p-replete/O₂ samples. The $g = 4.3$ signal arises from magnetically isolated Fe³⁺ species and not from ferric nanoparticles. This EPR region also exhibited the signals from the two high-spin Fe³⁺ heme centers (with $g = 4.6$, 5.3, and $g = 6.0$). Compared to the corresponding signals observed from Yah1p-replete/O₂ mitochondria, the concentrations of these species are *ca.* 50% lower. This is consistent with previous results showing that Yah1p is involved in heme *a* biosynthesis (11, 12), and with the known repression of heme synthesis under these conditions (7).

Electron Microscopy of Yah1p-Depleted/O₂ Mitochondria. The observation of nanoparticles by Mössbauer and EPR spectroscopy prompted us to collect STEM images as described in Experimental Procedures. In such images, brightness is directly related to the concentrations and atomic numbers of the contributing elements. High magnification STEM images of as-isolated Yah1p-depleted/O₂ mitochondria (Figure 5A) reveal bright punctate structures with diameters of 2–4 nm that associate into larger clumps. EDX spectra were collected within the boxed area, and transitions from C, Fe, O and P elements were observed. EDX mapping (Figure 5A) indicates that Fe, O and P concentrations maximize together (with roughly equimolar amounts of Fe and P, and a 10-fold molar excess of O) and colocalize with the punctate structures. Based on this analysis, as well as on the observed Mössbauer and EPR properties, we conclude that Fe in Yah1p-depleted mitochondria accumulates as 2–4 nm diameter ferric nanoparticles that weakly self-associate into larger clumps and are associated with phosphorus (as phosphate ions) and oxygen in roughly a Fe₁:P₁:O₁₀ molar ratio. Phosphate ions are present in mM concentration in the mitochondrial matrix (31). Further studies are required to establish the exact composition of this material.

Oxyblot Assay. The iron that accumulates in mitochondria of the Yah1p-depleted/O₂ cells is very similar, in terms of Mössbauer properties, to that in *yfh1* Δ mitochondria. Organelles from the latter mutant also contain nanoparticles, attributed to ferric phosphate (14). The homologous mutation in human fibroblasts reportedly accumulates mitochondrial nanoparticles in the form of ferrihydrite (32). We wondered whether these similarities extended to the effects on reactive oxygen production. Bulteau et al. (15) reported greater oxidative damage in *yfh1* Δ mitochondria than in WT mitochondria. To evaluate the relative extent of oxidative damage in our system, mitochondria isolated from Yah1p-replete/O₂ and Yah1p-depleted/O₂ cells were subjected to the Oxyblot assay. As shown in Figure 6, the extent of oxidatively carbonylated proteins in extracts of mitochondria isolated from Yah1p-depleted/O₂ cells (lane 2) is greater than that in equivalent extracts from Yah1p-replete/O₂ mitochondria (lane 4). This indicates that mitochondria depleted in Yah1p (from cells grown under an O₂ atmosphere) generate more reactive oxygen species than do mitochondria replete with Yah1p.

Treatment of Yah1p-Depleted/O₂ Mitochondria with Dithionite. After recognizing that the as-isolated sample of Yah1p-depleted/O₂ mitochondria contained ferric nanoparticles, we wondered to what extent the iron of these particles could be dissolved by treating intact mitochondria with a suitable reductant. To examine this, a sample of Yah1p-depleted/O₂ mitochondria was divided in two, and the control half was packed into a Mössbauer cup by centrifugation and then frozen. The other half was treated with dithionite as described in Experimental Procedures, and then packed by centrifugation (yielding also a supernatant fraction that was discarded in this experiment) and frozen. In both cases, the volume of the packed samples was \sim 250 μ L.

The control half (sample A) exhibited the spectra of Figure 2C,D, while the dithionite-treated sample (sample B) exhibited the 4.2 K spectrum of Figure 7A. The spectrum of sample B exhibited a new component representing 90% of Fe with $\Delta E_Q = 3.55(4)$ mm/s and $\delta = 1.33(2)$ mm/s. The

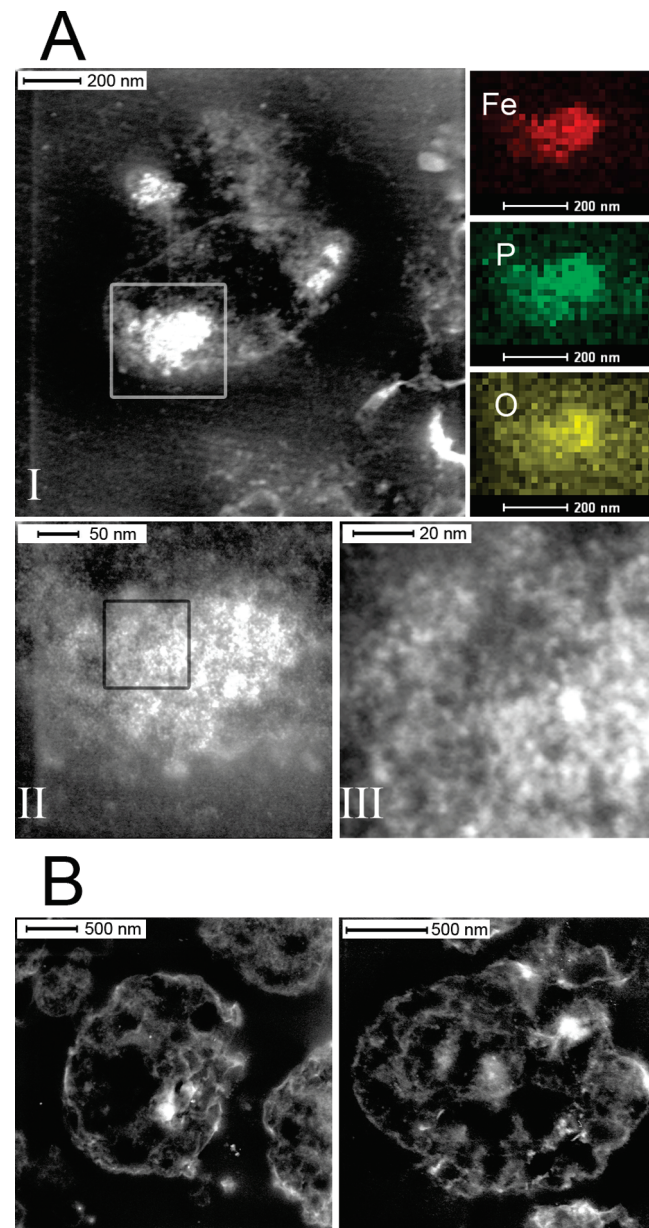


FIGURE 5: STEM-HAADF images of Yah1p-depleted/O₂ mitochondria in as-isolated (A) and dithionite-reduced (B) states. Image AIII is a magnified view of the region within the box shown in image AII. Image AII is a magnified view of the region within the box shown in AI. In these dark field images the contrast is reversed, so that a dark feature in a bright field transmission electron microscopy image may look bright. Those Z-contrast images collected from highly scattered electrons show distinct brightness in the high Z (atomic number) area with high spatial resolution. In addition, the combination of STEM and EDX also allows compositional analysis of a nanometer-scale area. In fact, when an EDX spectrum was obtained from the red-box area Fe, P, and O elements were the only clearly detected elements other than carbon. To see the spatial distribution of each element, elemental maps for Fe, P, and O are presented together after collection with a proper energy window assigned to the K α X-ray fluorescent transition of each element. They were acquired from a region similar but not identical to that within the box of image IA. In these pixelated elemental maps the brighter pixel indicates a higher concentration of the element. Therefore, comparison of the micrographs and the maps shows that the brightness in the STEM image is generally proportional to the concentration of the three elements.

nature of the remainder of the absorption is not clear, but it is not due to ferric nanoparticles. This doublet, with

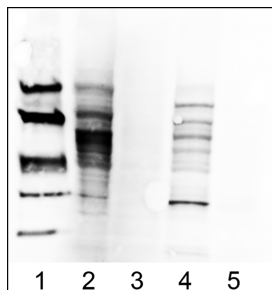


FIGURE 6: Oxyblot assay of Yah1p-depleted/O₂ and Yah1p-replete/O₂ SDS-solubilized mitochondrial extracts. From left to right: lane 1, Oxyblot molecular weight standards corresponding to (from top to bottom) 97.4, 68, 43, 29, and 21 kDa, respectively; lane 2, Yah1p-depleted/O₂; lane 3, Yah1p-depleted/O₂, negative control with no DNPH added; lane 4, Yah1p-replete/O₂; lane 5, Yah1p-replete/O₂, negative control with no DNPH added. Equivalent amounts (15 µg) of mitochondrial proteins were loaded onto lanes 2–5.

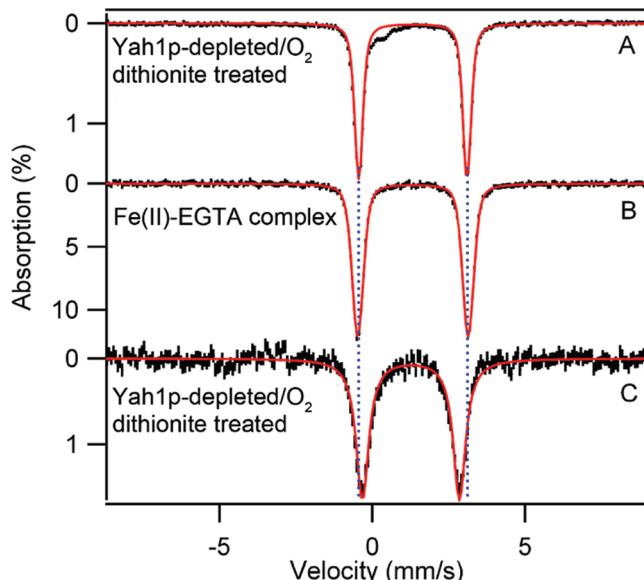


FIGURE 7: 4.2 Mössbauer spectra of dithionite-treated mitochondria (A, C) and Fe²⁺-EGTA complex (B) recorded in 40 mT magnetic field. (A) Dithionite-treated Yah1p-depleted/O₂ mitochondria (sample B), prepared in buffer containing EGTA; line width $\Gamma_V = 0.25$ mm/s. (B) Fe²⁺-EGTA complex in sorbital/tris buffer, as described in Experimental Procedures; $\Gamma_V = 0.40$ mm/s. (C) Dithionite-treated Yah1p-depleted/O₂ mitochondria in EGTA-free buffer; $\Gamma_V = 0.60$ mm/s. The solid lines are simulations assuming that the main feature is described by one quadrupole doublet. In all cases we have used Voigt profiles which assume distributions in ΔE_Q ; $\Gamma_V = 0.40$ mm/s is a Voigt shape obtained by convoluting a Lorentzian of 0.15 mm/s full width into a Gaussian of full width $\sigma_G = 0.40$ mm/s. Vertical lines mark the positions of the doublet in the top panel.

parameters characteristic of high-spin Fe²⁺, was observed in four separate experiments. The observation of one ferrous doublet with well-defined parameters suggests that the Fe²⁺ is bound in a specific complex, rather than to heterogeneous ligand environments as is often the case with adventitiously bound Fe²⁺.

Interestingly, as judged by Mössbauer spectroscopy the amount of total iron in sample B was 4-fold less than that observed in sample A. This suggests that ferrous ions are exported out of mitochondria during incubation with dithionite and then removed with the buffer in the centrifugation stage. Whether the Fe is exported through a leaky IM, possibly arising from an Fe-induced membrane permeability transition (33), or through an IM transporter is unknown.

We have attempted to identify the $\Delta E_Q = 3.55$ mm/s species. The parameters $\Delta E_Q = 3.55$ mm/s and $\delta = 1.33$ mm/s are unlike those observed for hexqua Fe²⁺ coordination environments; the latter typically yield $\Delta E_Q \approx 3.15$ –3.35 mm/s and $\delta \approx 1.38$ mm/s (34). This prompted us to test various components contained in the mitochondria or in the buffer used (see Supporting Information). Fe²⁺-phosphate and Fe²⁺-ATP complexes did not yield similar Mössbauer parameters. However, as shown in Figure 7B, EGTA-containing buffer gave a $\Delta E_Q \approx 3.62$ mm/s, $\delta \approx 1.33$ mm/s component, suggesting that the doublet observed in Figure 7A may arise from the Fe²⁺-EGTA complex. This interpretation is supported by the observation that dithionite-treated mitochondria lacked the $\Delta E_Q = 3.55$ mm/s species when EGTA was omitted from the buffer; instead, a doublet with $\Delta E_Q = 3.17(3)$ mm/s and $\delta = 1.26(1)$ mm/s was observed (Figure 7C). We cannot identify the coordinating ligand(s) of the $\Delta E_Q = 3.17$ mm/s species from Mössbauer parameters alone. EPR spectra of dithionite-treated Yah1p-depleted/O₂ mitochondria were also examined. Such samples essentially lacked the broad $g \approx 2$ resonance attributed to ferric nanoparticles (Figure 4B).

It has been reported that EGTA does not penetrate the mitochondrial IM (35). This would suggest that some or all of the species of Figure 7A is *external* to the mitochondria, perhaps contained in the buffer remaining after centrifugation following dithionite incubation. Indeed we have examined this supernatant fraction by Mössbauer spectroscopy and found that it contained high-spin Fe²⁺ ions. We have also studied the $\Delta E_Q = 3.55$ mm/s species observed in dithionite-treated mitochondria, as well as the Fe²⁺-EGTA buffer complex of Figure 7B, in strong applied magnetic fields (not shown). The high-field spectra of the Fe²⁺ components were quite similar and gave no indication that the Fe²⁺ species of Figure 7A,B are associated with nanoparticles.

STEM-HAADF images of dithionite-treated Yah1p-depleted/O₂ mitochondria also indicated substantially fewer nanoparticles (Figure 5B) and suggested that the resulting particulate material is dominated by phosphorus atoms (Fe:P ratio of 1:9). It would not be surprising if some residual nanoparticles remained after dithionite treatment, as our Mössbauer results suggest that the extent of reaction with dithionite is somewhat variable (60–100% reduction). The extents of reduction evident from the spectra shown in Figure 7A,C were the greatest achieved in our four attempts.

An EPR spectrum of dithionite-treated Yah1p-depleted/O₂ mitochondria is shown in Figure 4B. The spectrum lacks the broad EPR feature of Figure 4F, indicating that dithionite reduced the Fe³⁺ of the nanoparticles, but it exhibited an aqua-Mn²⁺ signal with the same intensity as observed in isolated Yah1p-depleted/O₂ mitochondria (Figure 4F). We suspect that the Mn²⁺ ions are located within the mitochondria, because they were not removed during isolation in EGTA-containing buffer. The presence of the Mn²⁺ signal in dithionite-treated and untreated mitochondria suggests that, in contrast to the behavior observed with Fe²⁺ ions, the Mn²⁺ ions are not displaced from the mitochondria upon treatment with dithionite. The chelator EGTA is also present in these samples, but it must not be interacting with the Mn²⁺ ions, since chelation of Mn²⁺ by EGTA would result in loss of the sharp 6-line hyperfine pattern at $g = 2$ (36). This suggests

that Fe^{2+} ions were not removed from dithionite-treated Yah1p-depleted/O₂ mitochondria due to a leaky IM.

The intensity of the $g_{\text{av}} = 2.005$ signal declined with dithionite-treatment (Figure 4B). Dithionite can penetrate phospholipid bilayer membranes and reduce species contained therein (37, 38); perhaps it reduced the species with $g_{\text{av}} = 2.005$. The corresponding region of an O₂-treated Yah1p-depleted/O₂ mitochondria sample lacked a strong $g_{\text{av}} = 2.005$ signal (Figure 4A), suggesting that this signal arises from species that can be oxidized into EPR-silent states.

Mössbauer and EPR Spectroscopy of Yah1p-Depleted/Ar Mitochondria. Iron is presumably imported into the mitochondria in the ferrous state (see introductory comments) suggesting that an oxidant is required to form ferric nanoparticles. To explore the possibility that the O₂ used in the cell growth was involved, we grew Gal-YAH1 cells using glucose as a carbon source (to repress the synthesis of Yah1p) under a strict argon atmosphere. In this case, the iron concentration of the isolated mitochondria was comparable to that of isolated Yah1p-replete/O₂ mitochondria and ~6-fold less than that of Yah1p-depleted/O₂ mitochondria. Thus, excess Fe did not accumulate when Yah1p-depleted cells were grown anaerobically. The 4.2 K Mössbauer spectrum of Yah1p-depleted/Ar mitochondria (Figure 2B) also indicated an ⁵⁷Fe concentration 8-to-10-fold less than that observed for Yah1p-depleted/O₂ mitochondria, but similar to that of Yah1p-replete/O₂ mitochondria. The difference in these fold-reductions may reflect differences in the methods (ICP-MS or Mössbauer) used. As seen in Figure 2B, ~60% of the Mössbauer absorption belongs to a group of doublets with parameters typical of high-spin Fe²⁺. One doublet, with $\Delta E_Q \approx 3.6$ mm/s (solid line in Figure 2B), might arise from the Fe²⁺-EGTA complex residing in the buffer, though this requires further investigation. Most, if not all, of the remaining iron in the sample belongs to unidentified ferric species. The spectrum of Figure 2B provides no evidence for ferric nanoparticles or [Fe₄S₄]²⁺ clusters; if present, they account for no more than 10% and 15% of the total Fe, respectively.

At 10 K, as-isolated Yah1p-depleted/Ar mitochondria exhibited an EPR spectrum in the high-field region (Figure 3D) that is similar to that of WT mitochondria (see Figure 6A of ref 19), but with more than a 10-fold decrease in the intensity of all signals. The spectrum is not dominated by the $g = 2.005$ radical signal. The $g_{\text{av}} = 1.94$ signal ([Fe₂S₂]¹⁺ cluster of succinate dehydrogenase) is 2-fold less intense than in spectra of Yah1p-replete/O₂ mitochondria. This suggests that Fe/S cluster assembly is attenuated under anaerobic growth conditions in Yah1p-depleted mitochondria. The resonance at $g = 2.03$ appears to have a contribution from oxidized [Fe₃S₄]¹⁺ clusters (<0.5 μM).

In the low-field region (Figure 3G), the spectrum shows signals from heme centers in similar amounts (~5 μM) to that of Yah1p-replete/O₂ mitochondria (Figure 3E), suggesting that hemes are present in mitochondria from Gal-YAH1 cells grown under anaerobic conditions. This is unexpected, because heme biosynthesis is O₂-dependent and transcriptionally repressed under low O₂ pressures (4). Several studies (39–41) suggest that anaerobically grown yeast cells synthesize a considerable amount of heme and hemoproteins, comparable in some reports to that synthesized under aerobic conditions. Trace amounts of O₂ could have been present

during the growth or harvesting of these nominally anaerobic cells, and such minuscule amounts might have been sufficient for heme synthesis (39). Interestingly, additional new signals are observed at $g = 4.9$ and 3.6. Signals in this region are not common, and at present we are unable to assign them. Simulations suggest that the resonances originate from an S = 5/2 system with E/D = 0.23, and if so, the concentration of this species would be ~3 μM .

DISCUSSION

In this study we have characterized mitochondria from the Gal-YAH1 strain of *S. cerevisiae* using EPR and Mössbauer spectroscopy, focusing on the Fe that accumulates when the strain is grown on glucose/O₂. When grown in this manner, cells are depleted in Yah1p, a ferredoxin required for Fe/S cluster assembly. Our results show that the mitochondria in these cells accumulate Fe in the form of aggregated ferric nanoparticles that contain iron and phosphate ions in approximately equimolar amounts. Nanoparticles with the same ΔE_Q and δ values were observed for *yfh1* Δ and were previously assigned to ferric phosphate. The exact composition of this material remains uncertain, but ferrihydrites tend to have somewhat larger ΔE_Q values, 0.67–0.85 mm/s, and smaller δ values, \approx 0.48 mm/s, than were observed. When the same strain is grown on galactose, cells are replete with Yah1p and thus serve as a control in our study. We have no evidence for the presence of accumulated Fe³⁺ nanoparticles in the mitochondria isolated from these cells; if present they would account for <8% of the total Fe.

Reducibility of Nanoparticles. Upon removal of O₂ and incubation of mitochondria in dithionite-containing buffer, the ferric nanoparticles were reductively dissolved. We are unaware of published reports indicating that the precipitated material in any other strain (e.g., *yfh1* Δ) could be reduced, but we suspect that it can. The ability to reduce this material in Yah1p-depleted/O₂ mitochondria shows a potential efficacy of removing precipitated Fe³⁺ by reductive dissolution at the particle surface and then chelating the more soluble Fe²⁺ form from the cytosol. Kaplan and co-workers have reported that the aggregated material in mitochondria from Yfh1p-depleted cells can be eliminated by expressing *YFH1* (42), suggesting that Yfh1p directly or indirectly promotes the reduction of the aggregated material and its export from or utilization by the mitochondria.

Similarity to the *yfh1* Δ Phenotype. The Fe that accumulates as ferric nanoparticles in mitochondria of Yah1p-depleted/O₂ cells has the same Mössbauer spectrum, within the signal/noise, as that observed in mitochondria from *yfh1* Δ cells (14). Another aspect of what appears to be a shared phenotype is an increase in oxidative damage, relative to WT cells, as evidenced by the results of the Oxyblot assay reported here and elsewhere (15). These two mitochondrial proteins function at different stages in Fe/S cluster assembly, but both act upstream of reactions involving the later stages of assembly and/or release of Fe/S clusters by scaffold proteins Isu1/2p. It is unlikely that the accumulation and aggregation arise from a blockage of heme biosynthesis, since disrupting the heme biosynthesis pathway in yeast does not cause Fe to accumulate (43). Rather, these common phenotypic effects probably arise from distinct malfunctions, one involving Yah1p and the other involving Yfh1p, that both block Fe/S cluster assembly.

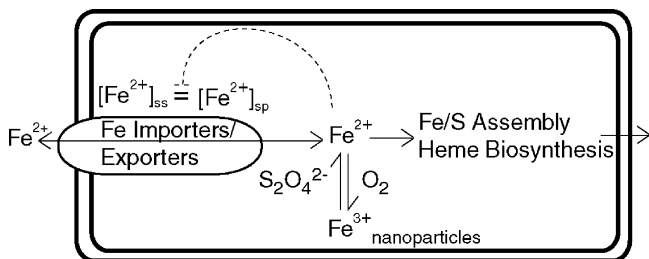


FIGURE 8: Scheme for explaining the accumulation of ferric nanoparticles in mitochondria from Yah1p-depleted/O₂ and *yfh1*Δ cells. See text for details.

Excess Iron Accumulation Is O₂ Dependent. Iron is imported into the mitochondria in the 2+ state (44), but the Fe which accumulates occurs in the form of Fe³⁺ nanoparticles, suggesting that the imported Fe²⁺ must become oxidized to the Fe³⁺ state before it aggregates. Fe³⁺ nanoparticles accumulate only in mitochondria from Gal-YAH1 cells that are both depleted in Yah1p and grown under aerobic conditions. The absence of Fe accumulation in mitochondria from Yah1p-depleted/Ar cells indicates that accumulation requires both a deficiency of Yah1p (or Yfh1p) and exposure to O₂ during cell growth. We conclude that the accumulation of Fe depends, either directly or indirectly, on the prior oxidation of Fe²⁺ to Fe³⁺.

Has the Regulation of Fe Import Gone Awry in Yah1p-Depleted Mitochondria? Although many details of the homeostatic Fe regulatory mechanism in mitochondria remain to be clarified, we consider the general scheme shown in Figure 8. Accordingly, the concentration of Fe²⁺ ions in the matrix is presumed to be sensed by IM Fe transporters (dashed line). If the steady-state concentration of Fe²⁺ ([Fe²⁺]_{ss}) equals some optimal set-point concentration ([Fe²⁺]_{sp}), the IM Fe transporter imports Fe²⁺ at a modest, regulated rate. When [Fe²⁺]_{ss} > [Fe²⁺]_{sp}, the rate of Fe²⁺ import decreases; when [Fe²⁺]_{ss} < [Fe²⁺]_{sp}, the rate increases. A similar regulatory mechanism could involve Fe exporters in the IM, which would respond oppositely to these comparative conditions.

Could the accumulation of Fe in *yah1p*-depleted and *yfh1*Δ cells be caused by a malfunction in this regulatory mechanism, such that the rate of Fe²⁺ import was “locked” at an excessive rate? Fe²⁺ ions did not accumulate in Yah1p-depleted/Ar cells, suggesting that the homeostatic mechanism for regulating mitochondrial Fe *does* function appropriately under Yah1p-depleted conditions, *as long as O₂ is excluded*. We also observed a substantial (75–90%) release of Fe²⁺ from the mitochondria following incubation in dithionite-containing buffer. Although we cannot exclude the possibility that the dithionite-induced increase in Fe²⁺ within the mitochondria caused the membrane to become leaky, it could also be that the condition [Fe²⁺]_{ss} > [Fe²⁺]_{sp} increased the rate of Fe²⁺ export. Considered collectively, our results suggest (but do not establish) that the absence of Yah1p (and by extension Yfh1p) does not cause a malfunction in the homeostatic Fe regulatory mechanism in mitochondria.

Why Do Ferric Nanoparticles Form in Yah1p-Depleted/O₂ (and *yfh1*Δ) Cells but Not in WT Cells? We suggest two explanatory models, one based on a difference in the coordination environment of the Fe^{2+/3+} ions in the mitochondrial matrix, the other based on a difference in the redox status of the matrix region in the presence of O₂. Aqueous

Fe³⁺ is highly insoluble (45), but the Fe³⁺ in oxidized mitochondria from respiring WT cells is not present in nanoparticles that exhibit a quadrupole doublet with ΔE_Q = 0.62 mm/s (19). We are uncertain whether the Fe³⁺ ions observed in WT mitochondria are located *within* the organelle, but if they are, it would appear that they have a coordination environment that prevents their precipitation. Fe³⁺ ions in Yah1p-depleted/O₂ (and *yfh1*Δ) mitochondria might lack such protection and thus precipitate, forming the Fe³⁺ nanoparticles observed here. The protective ligand may not be synthesized in these mutant strains, or the large amount of Fe³⁺ ions that develops might simply overwhelm the amount of protective ligand available. The former possibility would suggest that Yah1p (and Yfh1p) somehow promotes the synthesis of the protecting ligand, which seems unlikely. The latter possibility could be realized by the inability of these cells to synthesize Fe/S clusters. In this case, aqueous Fe²⁺ ions would build up; thus under oxidizing conditions, they would become oxidized to aqueous Fe³⁺ ions which would precipitate immediately.

The second explanatory model assumes that the Fe³⁺ observed in WT mitochondria (19) is adventitiously bound to proteins or membranes on the exterior of the organelle. This model further assumes that, in WT cells, the mitochondrial matrix region remains largely “reducing” in terms of electrochemical potential, *even when cells are grown in an O₂ atmosphere* (and when anaerobically isolated mitochondria are briefly exposed to O₂, as we have done (19)). This assumption is supported by the Oxyblot results reported here and elsewhere (15), which indicate higher oxidative stress in these mutant cells. According to this model, the reducing environment of the matrix in WT cells minimizes iron oxidation such that the concentration of Fe³⁺ does not exceed its solubility limit. In mutant mitochondria, the more oxidizing matrix environment increases [Fe³⁺] beyond its solubility limit, and the ions precipitate. The mechanisms by which WT cells establish such a reduced matrix and that by which the mutant cells disestablish it are beyond the scope of this model. However, it does not appear as simple as abolishing oxidative phosphorylation (e.g., by blocking the synthesis of Fe/S clusters and hemes) because there are examples in which such abolition in yeast does not cause Fe accumulation (46, 47). We view this as evidence against this model, but perhaps not sufficient to discard it. The concept of oxidative stress is sufficiently vague that there may be other unidentified mechanisms for establishing whether the matrix is oxidizing or reducing.

Apart from these differences, the mechanism of ferric nanoparticle formation is the same for both models. In Yah1p-depleted/O₂ or *yfh1*Δ mitochondria, either the absence of a “protecting” ligand or the presence of a more oxidizing matrix environment leads to the formation of Fe³⁺ followed by precipitation. As these ions precipitate the equilibrium shifts toward Fe³⁺. This, in turn, affords the condition [Fe²⁺]_{ss} < [Fe²⁺]_{sp}, which activates Fe importers (or deactivates Fe exporters), resulting in the observed accumulation of Fe. According to these models, the presence of ferric nanoparticles is *not* sensed by the IM Fe transporters, so the buildup of this material proceeds without perturbing the regulatory sensing condition. In the absence of O₂, the equilibrium is *not* shifted toward Fe³⁺ such that the condition [Fe²⁺]_{ss} ≈ [Fe²⁺]_{sp} holds and the Fe transporters import Fe²⁺ at a

regulated rate. In the presence of dithionite (and absence of O₂), the precipitated material is reductively dissolved such that [Fe²⁺]_{ss} > [Fe²⁺]_{sp}, and the transporters export Fe²⁺ at an increased rate.

Both models, and the regulatory mechanism that was assumed to develop them, require extensive additional testing. For example, the concentration of other Fe species besides matrix-bound [Fe²⁺] may be sensed, and other species besides IM transporters may be regulated. Nevertheless, these models represent a testable molecular-level description for the formation of the ferric nanoparticles. Understanding the molecular basis for the formation of these nanoparticles in Yah1p-depleted/O₂ and *yfh1* Δ cells may ultimately contribute to a more in-depth understanding of Friedreich's ataxia. One obvious test would be to identify the ligands coordinating Fe²⁺/Fe³⁺ ions in WT mitochondria and in the Fe²⁺ ions obtained by treating ferric nanoparticles with dithionite. Such experiments are underway.

ACKNOWLEDGMENT

We thank Professor Cristine Heaps (School of Veterinary Medicine, Texas A&M University) for use of her imager, Dr. Audria Stubna for collecting initial Mössbauer spectra, and Mr. Greg Holmes-Hampton for help with the OxyBlot assays.

SUPPORTING INFORMATION AVAILABLE

Table of Mössbauer parameters of various Fe(II) complexes relevant to this study. This material is available free of charge via the Internet at <http://pubs.acs.org>.

REFERENCES

- Lill, R., and Mühlenhoff, U. (2006) Iron-sulfur protein biogenesis in eukaryotes: Components and mechanisms. *Annu. Rev. Cell. Dev. Biol.* 22, 457–486.
- Lill, R., Dutkiewicz, R., Elsasser, H. P., Hausmann, A., Netz, D. J. A., Pierik, A. J., Stehling, O., Urzica, E., and Mühlenhoff, U. (2006) Mechanisms of iron-sulfur protein maturation in mitochondria, cytosol and nucleus of eukaryotes. *Biochim. Biophys. Acta Mol. Cell Res.* 1763, 652–667.
- Kwok, E., and Kosman, D. (2006) Iron in yeast: Mechanisms involved in homeostasis, in *Molecular Biology of Metal Homeostasis and Detoxification: From Microbes to Man* (Tamás, M. J., and Martinoia, E., Eds.), pp 59–99, Springer, Berlin.
- Rosenfeld, E., and Beauvoit, B. (2003) Role of the non-respiratory pathways in the utilization of molecular oxygen by *Saccharomyces cerevisiae*. *Yeast* 20, 1115–1144.
- Mühlenhoff, U., Stadler, J. A., Richhardt, N., Seubert, A., Eickhorst, T., Schweyen, R. J., Lill, R., and Wiesenberger, G. (2003) A specific role of the yeast mitochondrial carriers Mrs3/4p in mitochondrial iron acquisition under iron-limiting conditions. *J. Biol. Chem.* 278, 40612–40620.
- Lange, H., Mühlenhoff, U., Denzel, M., Kispal, G., and Lill, R. (2004) The heme synthesis defect of mutants impaired in mitochondrial iron-sulfur protein biogenesis is caused by reversible inhibition of ferrochelatase. *J. Biol. Chem.* 279, 29101–29108.
- Hausmann, A., Samans, B., Lill, R., and Mühlenhoff, U. (2008) Cellular and mitochondrial remodeling upon defects in iron-sulfur protein biogenesis. *J. Biol. Chem.* 283, 8318–8330.
- Mühlenhoff, U., Gerber, J., Richhardt, N., and Lill, R. (2003) Components involved in assembly and dislocation of iron-sulfur clusters on the scaffold protein Isu1p. *EMBO J.* 22, 4815–4825.
- Barros, M. H., and Nobrega, F. G. (1999) YAH1 of *Saccharomyces cerevisiae*: a new essential gene that codes for a protein homologous to human adrenodoxin. *Gene* 233, 197–203.
- Lange, H., Kaut, A., Kispal, G., and Lill, R. (2000) A mitochondrial ferredoxin is essential for biogenesis of cellular iron-sulfur proteins. *Proc. Natl. Acad. Sci. U.S.A.* 97, 1050–1055.
- Barros, M. H., Nobrega, F. G., and Tzagoloff, A. (2002) Mitochondrial ferredoxin is required for heme A synthesis in *Saccharomyces cerevisiae*. *J. Biol. Chem.* 277, 9997–10002.
- Barros, M. H., Carlson, C. G., Glerum, D. M., and Tzagoloff, A. (2001) Involvement of mitochondrial ferredoxin and Cox15p in hydroxylation of heme O. *FEBS Lett.* 492, 133–138.
- Babcock, M., deSilva, D., Oaks, R., DavisKaplan, S., Jiralerpong, S., Montermini, L., Pandolfo, M., and Kaplan, J. (1997) Regulation of mitochondrial iron accumulation by Yfh1p, a putative homolog of frataxin. *Science* 276, 1709–1712.
- Lesuisse, E., Santos, R., Matzanke, B. F., Knight, S. A. B., Camadro, J. M., and Dancis, A. (2003) Iron use for haeme synthesis is under control of the yeast frataxin homologue (Yfh1). *Hum. Mol. Genet.* 12, 879–889.
- Bulteau, A. L., Dancis, A., Gareil, M., Montagne, J. J., Camadro, J. M., and Lesuisse, E. (2007) Oxidative stress and protease dysfunction in the yeast model of Friedreich ataxia. *Free Radical Biol. Med.* 42, 1561–1570.
- Aisen, P., Enns, C., and Wessling-Resnick, M. (2001) Chemistry and biology of eukaryotic iron metabolism. *Int. J. Biochem. Cell Biol.* 33, 940–959.
- Rotig, A., deLonlay, P., Chretien, D., Foury, F., Koenig, M., Sidi, D., Munnich, A., and Rustin, P. (1997) Aconitase and mitochondrial iron-sulphur protein deficiency in Friedreich ataxia. *Nat. Genet.* 17, 215–217.
- Chaston, T. B., and Richardson, D. R. (2003) Iron chelators for the treatment of iron overload disease: Relationship between structure, redox activity, and toxicity. *Am. J. Hematol.* 73, 200–210.
- Hudder, B. N., Garber, J. M., Stubna, A., Münck, E., Hendrich, M. P., and Lindahl, P. A. (2007) Electron paramagnetic resonance and Mössbauer spectroscopy of intact mitochondria from respiring *Saccharomyces cerevisiae*. *J. Biol. Inorg. Chem.* 12, 1029–1053.
- Kushnirov, V. V. (2000) Rapid and reliable protein extraction from yeast. *Yeast* 16, 857–860.
- Watters, C. (1978) One-step Biuret assay for protein in presence of detergent. *Anal. Biochem.* 88, 695–698.
- Parvin, R., Pande, S. V., and Venkitas, Ta. (1965) On colorimetric Biuret method of protein determination. *Anal. Biochem.* 12, 219–229.
- Yeast genome database: <http://www.yeastgenome.org/straitable.shtml>.
- Dedeken, R. H. (1966) Crabtree effect—a regulatory system in yeast. *J. Gen. Microbiol.* 44, 149–156.
- Kwast, K. E., Lai, L. C., Menda, N., James, D. T., Aref, S., and Burke, P. V. (2002) Genomic analyses of anaerobically induced genes in *Saccharomyces cerevisiae*: Functional roles of Rox1 and other factors in mediating the anoxic response. *J. Bacteriol.* 184, 250–265.
- Battle, P. D., Cheetham, A. K., Gleitzer, C., Harrison, W. T. A., Long, G. J., and Longworth, G. (1982) A novel magnetic phase transition in anhydrous iron(III) phosphate, FePO₄. *J. Phys. C: Solid State Phys.* 15, L919–L924.
- StPierre, T. G., Chan, P., Bauchspies, K. R., Webb, J., Betteridge, S., Walton, S., and Dickson, D. P. E. (1996) Synthesis, structure and magnetic properties of ferritin cores with varying composition and degrees of structural order: Models for iron oxide deposits in iron-overload diseases. *Coord. Chem. Rev.* 151, 125–143.
- Bauminger, E. R., Cohen, S. G., Dekanter, F. L., Levy, A., Ofer, S., Kessel, M., and Rottem, S. (1980) Iron storage in *Mycoplasma capricolum*. *J. Bacteriol.* 141, 378–381.
- Weir, M. P., Peters, T. J., and Gibson, J. F. (1985) Electron-spin resonance studies of splenic ferritin and hemosiderin. *Biochim. Biophys. Acta* 828, 298–305.
- Wajnberg, E., El-Jaick, L. J., Linhares, M. P., and Esquivel, D. M. S. (2001) Ferromagnetic resonance of horse spleen ferritin: Core blocking and surface ordering temperatures. *J. Magn. Reson.* 153, 69–74.
- Rauen, U., Springer, A., Weisheit, D., Petrat, F., Korth, H. G., de Groot, H., and Sustmann, R. (2007) Assessment of chelatable mitochondrial iron by using mitochondrion-selective fluorescent iron indicators with different iron-binding affinities. *ChemBioChem* 8, 341–352.
- Popescu, B. F. G., Pickering, I. J., George, G. N., and Nichol, H. (2007) The chemical form of mitochondrial iron in Friedreich's ataxia. *J. Inorg. Biochem.* 101, 957–966.
- Rauen, U., Petrat, F., Sustmann, R., and de Groot, H. (2004) Iron-induced mitochondrial permeability transition in cultured hepatocytes. *J. Hepatol.* 40, 607–615.

34. Kalman, E., Radnai, T., Palinkas, G., Hajdu, F., and Vertes, A. (1988) Hydration of iron(II) ion in aqueous-solutions. *Electrochim. Acta* 33, 1223–1228.
35. Virag, L., Scott, G. S., Antal-Szalmás, P., O'Connor, M., Ohshima, H., and Szabo, C. (1999) Requirement of intracellular calcium mobilization for peroxynitrite-induced poly(ADP-ribose) synthetase activation and cytotoxicity. *Mol. Pharmacol.* 56, 824–833.
36. Reed, G. H., Leigh, J. S., and Pearson, J. E. (1971) Electron paramagnetic relaxation and epr line shapes of manganous ion complexes in aqueous solutions - frequency and ligand dependence. *J. Chem. Phys.* 55, 3311–3316.
37. Langner, M., and Hui, S. W. (1993) Dithionite penetration through phospholipid -bilayers as a measure of defects in lipid molecular packing. *Chem. Phys. Lipids* 65, 23–30.
38. McIntyre, J. C., and Sleight, R. G. (1991) Fluorescence assay for phospholipid membrane asymmetry. *Biochemistry* 30, 11819–11827.
39. Zagorec, M., Buhler, J. M., Treich, I., Keng, T., Guarente, L., and Labbebois, R. (1988) Isolation, sequence, and regulation by oxygen of the yeast Hem-13 gene coding for coproporphyrinogen oxidase. *J. Biol. Chem.* 263, 9718–9724.
40. Camadro, J. M., Thome, F., Brouillet, N., and Labbe, P. (1994) Purification and properties of protoporphyrinogen oxidase from the yeast *Saccharomyces cerevisiae*—mitochondrial location and evidence for a precursor form of the protein. *J. Biol. Chem.* 269, 32085–32091.
41. Buisson, N., and Labbe-Bois, R. (1998) Flavohemoglobin expression and function in *Saccharomyces cerevisiae*—No relationship with respiration and complex response to oxidative stress. *J. Biol. Chem.* 273, 9527–9533.
42. Radisky, D. C., Babcock, M. C., and Kaplan, J. (1999) The yeast frataxin homologue mediates mitochondrial iron efflux—Evidence for a mitochondrial, iron cycle. *J. Biol. Chem.* 274, 4497–4499.
43. Crisp, R. J., Pollington, A., Galea, C., Jaron, S., Yamaguchi-Iwai, Y., and Kaplan, J. (2003) Inhibition of heme biosynthesis prevents transcription of iron uptake genes in yeast. *J. Biol. Chem.* 278, 45499–45506.
44. Lange, H., Kispal, G., and Lill, R. (1999) Mechanism of iron transport to the site of heme synthesis inside yeast mitochondria. *J. Biol. Chem.* 274, 18989–18996.
45. Boukhalfa, H., and Crumbliss, A. L. (2002) Chemical aspects of siderophore mediated iron transport. *BioMetals* 15, 325–339.
46. Chen, O. S., Hemenway, S., and Kaplan, J. (2002) Inhibition of Fe-S cluster biosynthesis decreases mitochondrial iron export: Evidence that Yfh1p affects Fe-S cluster synthesis. *Proc. Natl. Acad. Sci. U.S.A.* 99, 12321–12326.
47. Chen, O. S., and Kaplan, J. (2001) YFH1-mediated iron homeostasis is independent of mitochondrial respiration. *FEBS Lett.* 509, 131–134.

BI801047Q